

RADIUS INFLATION AT LOW ROSSBY NUMBER IN THE HYADES CLUSTER

KARL JAEHNIG^{1,2}, GARRETT SOMERS^{2,3}, AND KEIVAN G. STASSUN^{2,1}

¹Department of Physics, Fisk University, Nashville, TN, 37208, USA

²Department of Physics and Astronomy, Vanderbilt University, Nashville, TN 37235, USA

³Vanderbilt Initiative in Data-intensive Astrophysics Fellow

ABSTRACT

Radius inflation continues to be explored as a peculiar occurrence among magnetically active, low-mass stars. Recently Somers & Stassun (2017) showed that radius inflation among low-mass stars in the young open cluster M45 (Pleiades Cluster) is correlated to the rotation rate: faster rotators are more inflated. Here we extend that work to a sample of 68 stars of the older open Hyades Cluster. We employ spectral energy distribution fitting to derive bolometric flux. With spectroscopically defined T_{eff} , and Gaia DR2 distances we calculate stellar radii using the Stefan-Boltzmann equation. We find numerous stars that exhibit significant ($3-4\sigma$) radius inflation relative to a nominal cluster isochrone. We compare these results to that of the younger Pleiades and consider radius inflation as a function of open cluster evolution. We find that unlike the Pleiades, there is not a statistically significant correlation between radius inflation and stellar rotation period. However, we do find that most inflated stars have (rapid) rotational Rossby numbers of 0.1–0.2, such that the correlation of radius inflation with Rossby number is statistically significant with 99.98% confidence. Our results imply that magnetic activity within the convective layers of low-mass stars preferentially drives radius inflation.

Keywords: Astrophysics - Solar and Stellar Astrophysics

1. INTRODUCTION

A consensus is emerging that some low-mass stars ($M \lesssim 1M_{\odot}$) have larger radii than expectations from standard stellar theory. This so-called “radius inflation” effect is typically of order 10–15% and is correlated with a roughly 5–10% lower effective temperature than predicted. Radius inflation has been observed in numerous studies using a variety of observational techniques including eclipsing binary analysis (e.g. Popper 1997; Torres & Ribas 2002; López-Morales & Ribas 2005), statistical projected radii (e.g. Jackson et al. 2016, 2018), and spectral energy distribution (SED) fitting Somers & Stassun (2017, S2017 hereafter). Though the precise mechanism is still debated, strong magnetic activity seems to play a role either through the direct inhibition of convective energy transport, the influence of large starspots on the photospheric pressure and temperature, or a combination of both effects (e.g. Mullan & MacDonald 2001; Chabrier, Gallardo & Baraffe 2007; Macdonald & Mullan 2010; Feiden & Chaboyer 2013, 2014; Jackson & Jeffries 2014a,b; Somers & Pinsonneault 2014, 2015b,a). This conclusion is based on observed correlations between radius inflation and proxies of magnetic activity such as H_{α} emission, X-rays, and rotation rate (e.g. López-Morales & Ribas 2005; Stassun et al. 2012; Somers & Stassun 2017).

S2017 investigated whether any of the single K-dwarfs in the young Pleiades open cluster showed evidence of radius

inflation. By fitting the individual SEDs to measure the luminosity of each member, measuring their effective temperature using color proxies, and solving the Stefan-Boltzmann equation, S2017 determined the radii of 80+ Pleiads and compared them to stellar evolution models. They found that for stars rotating slower than a two day period, corresponding to a Rossby number (R_N) greater than ~ 0.1 in the mass range they studied ($\sim 0.7 - 0.9M_{\odot}$), the models predicted the Teff-radius relation extremely well. However, stars rotating faster than 2 days ($R_N \lesssim 0.1$) were on average $\sim 12\%$ larger than predicted. This is an interesting value of R_N – numerous other studies have found that the correlation between rotation rate and magnetic proxies saturates at approximately this value (e.g. Wright et al. 2011). This suggests that the radius inflation mechanism may be connected to the as-yet unclear physics of magnetic saturation. Moreover, these inflated Pleiads tended to show higher lithium abundances as expected from stars experiencing radius inflation during their early lives (e.g. Somers & Pinsonneault 2014, 2015b,a).

Following the success of this study, we now wish to explore the time-dependent evolution of radius inflation. If radius inflation is a consequence of magnetic activity and rapid rotation, it stands to reason that the degree of radius inflation at fixed spectral type should decline with increasing age as stars both spin down and become less magnetically active (e.g. Skumanich 1972). If in fact radius inflation exists for

stars with Rossby numbers below about 0.1 as suggested by the results of S2017, then the masses of inflated stars will be lower on average in older clusters, owing to the slower spin down rate of less massive stars. As a complement to the Pleiades, this paper will focus on the Hyades.

The structure of the paper is as follows: In section 2.1 we discuss the data we collected to form a complete sample of the Hyades pre-main sequence stars as well as any relevant data quality measures that were employed. In section 3 we detail how we calculated the radius inflation for each star in the Hyades. In section 4 we present the results we found between the derived radii inflation within the Hyades and stellar rotation of the stars. In section 5 we discuss the implications of our results with respect to stellar evolution and with regard to previous work in radii inflation. We present a summary of our findings in section 6

2. DATA

2.1. The Hyades sample

2.1.1. Source Catalogs

In order to properly derive effective temperatures for the stars within the Hyades, it is necessary to build a sample of known members and their magnitude measurements in different bands. We start with the Hyades membership list from the (Goldman et al. 2013, hereafter G2013) catalog. G2013 made use of Pan-STARRS (Chambers et al. 2016) and PPMXL (Roeser et al. 2010) photometry, complimented by photometry from 2MASS (Skrutskie et al. 2006), SDSS-III DR8 (Aihara et al. 2011), and UKIDSS DR8 (Lawrence et al. 2007), in order to construct a complete stellar mass function. The G2013 final sample size of Hyades member stars was 774. The G2013 catalog did not have rotational periods for its final sample of Hyades stars and so it is necessary to complement the G2013 photometry with other catalogues which included rotation measurements.

To this end we employ two catalogues which have Hyades member stars with measured rotational periods. (Douglas et al. 2016, hereafter D2016) measured rotation periods for 65 Hyades stars using the Kepler spacecraft during its K2 phase in order to study low-mass star gyrochronology. We cross-matched the D2016 sample against the 2MASS catalog in order to find complimentary stars within the G2013 catalog. We find that all 65 of the D2016 Hyades stars have cross-matches within the G2013 catalog.

(Delorme et al. 2011, hereafter D2011) also measured rotation periods for 63 Hyades stars in order to also study gyrochronology within the Hyades. Cross-matching the D2011 catalog with 2MASS we find 59 Hyades stars that have complimentary observations within the G2013 catalog. Within this set of 122 stars we check for stars with double observations, finding 13 stars that have observations in both D2011 and D2016, thus reducing our initial sample to 109 stars. We plot the color-magnitude diagram of this sample in Figure 1.

Having compiled a set of Hyades members with measured periods, we move to collect photometry in order to calculate the T_{eff} . We query the SIMBAD database (Wenger et al. 2000) in order to gather photometry in the Johnson passbands ($UBVR_J I_J JHK$). Following the assumptions laid out

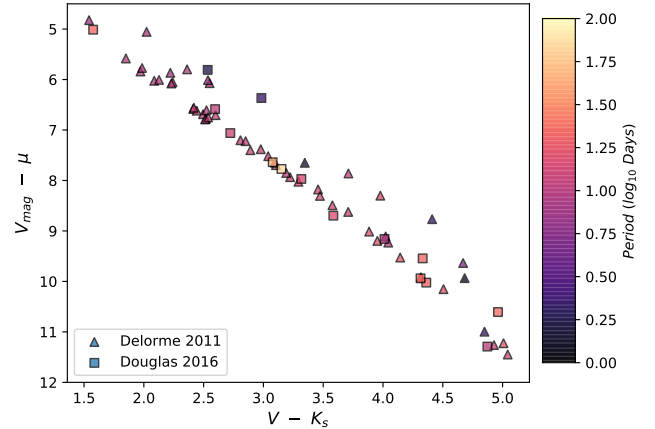


Figure 1. Color-magnitude diagram of the Hyades sample used in this work. Triangles are sources taken from Delorme et al. (2011) and squares are sources taken from Douglas et al. (2016). The points are all colored by their period in \log_{10} days.

by Somers & Stassun (2017), we attempt to collect V and I_c photometry as this will provide a precise upper limit on the T_{eff} , and therefore a precise lower limit on radius. With a precise lower limit on the radius, it is possible to detect variations on the stellar radius caused by radius inflation. Unfortunately, as S2017 found a dearth of measurements in the I_c band for the Pleiades, we too found a dearth of I_c measurements for the Hyades stars. We find that there is sufficient V, and K_s 2MASS photometry to calculate T_{eff} using the V- K_s color. We cross-matched 2MASS ids with CDS to download the K_s magnitudes and use the V magnitudes from Johnson & Knuckles (1955) in order to assemble our sample of colors for the Hyades stars.

2.1.2. Binaries within our Hyades Sample

When it comes to the study of radius inflation in single stars, binaries pose a problem, as they can produce false indications of radius inflation photometrically. This problem arises from the additional flux from an unresolved binary system, causing observations to result in a higher measured magnitude. Typically, photometric binaries are identified because they form their own main sequence above the single star main sequence in the color-magnitude diagram. This effect has already been explored by S2017 who searched for, and excluded binaries within their Pleiades sample. We summarize their conclusions of the effects of binaries on radii inflation below:

- Equal mass binaries will increase bolometric flux without significantly affecting the measured T_{eff} , thus leading to a significant signal of radius inflation
- For low-mass-ratio binaries, the total bolometric flux is barely affected but the near-IR emission is significantly boosted, leading to a lower inferred T_{eff} calculation. This can result in a false signal of radius inflation because the lower inferred temperatures means the star will be compared to the radius predicted for a lower-mass star.

We proceed to look through our sample of Hyads for binary systems that have been confirmed with previous surveys. We focus primarily on finding confirmation either through spectroscopic surveys, which involve measuring the radial velocity and possible calculation of the orbital elements, or optical surveys where the binary is resolved and its motions can be calculated.

As the Hyades is among the most observed open clusters, it is not difficult to find several surveys that considered both cluster membership, as well as binarity. For our sample of Hyads we consult [Kopytova et al. \(2016\)](#) for an initial list of their identified single stars, as well as the works they used to exclude stars that were in binary systems. We construct a list of confirmed multiple systems using the catalogs of [Mermilliod, Mayor & Udry \(2009\)](#), [Patience et al. \(1998\)](#), and [Duchêne et al. \(2013\)](#). From which we find a total of 349 stars that have been identified as single to the best of our ability. Within this sample of single stars we find that 45 stars within our sample of 68 Hyads have been previously identified as single stars.

For the other 23 stars within our sample we query *Vizier* for any catalogues in which the binary status has been confirmed. We find that 20 of our 23 Hyads are confirmed binaries, with observations coming from the Tycho Double Star Catalog ([Fabricius, Høg, Makarov, Mason, Wycoff & Urban 2002](#)), the Washington Double Star Catalog ([Mason, Wycoff, Hartkopf, Douglass & Worley 2001](#)), [Douglas, et al. \(2014\)](#), and [Bobylev 2016](#). We cannot find confirmation of binarity, or single star status for three stars, and decide to exclude them from our analysis. The final binary status for our final sample can be found in the last column of table 1, where

- No - Confirmed Single Star
- Yes - Confirmed Binary System
- Yes? - Unconfirmed Binary/Single Star.

2.2. Pleiades Sample

The constraints applied to the data that we have just described largely follow the same conventions employed by S2017 in their analysis of the Pleiades cluster. In the following sections we outline our methods in analyzing our sample of Hyads. We have also introduce a novel method for calculating stellar radius inflation that takes into account the relationship between changes in T_{eff} and radius (See section 3.4).

We want to compare our results to the Pleiades results from S2017, but their method for determining ΔR did not account for this relationship. Instead, they simply used the isochronal radius at the measured T_{eff} of the star as a comparison point. A direct comparison with their values would therefore be biased. Instead, we recompute radius inflation for the Pleiades using the methods we have developed in section 3.4.

3. METHODS

Using the well know Stefan-Boltzmann law

$$L = 4\pi R_*^2 \sigma_{SB} T_{\text{eff}}^4, \quad (1)$$

the radius of a star can be derived if its luminosity and T_{eff} are known with acceptable precision. The luminosity can be determined using the equation

$$L = 4\pi d^2 f_{\text{bol}}, \quad (2)$$

where f_{bol} is the bolometric flux and d is the distance to the star. The T_{eff} calculation remains the most crucial task in studying radius inflation, as it is the biggest contributor to the final uncertainty in the calculated radius ($R \propto L^{1/2} \cdot T^{-2}$). In the subsections that follow, we briefly go over the derivation of T_{eff} , the bolometric flux, and the stellar radii of our sample of Hyads, (see S2017).

3.1. Effective Temperature

In order to calculate T_{eff} using the V- K_s color we need to account for any possible extinction present in the Hyades. Since the Hyades is both within the local bubble and an older open cluster (650 ± 70 Myr ([Martín et al. 2018](#))), there is very little extinction arising within the cluster or in the intervening ISM. We adopt $E(B-V) = 0.01$ ([Gunn & Stryker 1983](#)), a typical value quoted for the Hyades. To convert this value to other colors, we employ the standard reddening law from [Cardelli et al. \(1989\)](#) with a selective reddening of $R_v = 3.1$. This gives us an $E(V-K_s)$ value of 0.027. With this we then proceed to use the empirical metallicity dependent calibrations from [Huang et al. \(2015\)](#) to calculate T_{eff} using V- K , adopting $[\text{Fe}/\text{H}] = 0.135$ ([Cummings+2012](#)). These color- T_{eff} calibrations are valid over a V- K_s color range of [0.85, 5.05]. With their calibrations we are able to derive T_{eff} values for 68 stars out of our initial sample of 109 Hyads. We provide the 2MASS ids, positions, photometric measurements, and measured rotation period in Table 1.

3.2. Bolometric Flux

In order to calculate the total bolometric flux of a star, f_{bol} , we fit the observed spectral energy distribution (SED) of each Hyades star with a standard stellar atmosphere model from [Kurucz \(2013\)](#). This is the same SED fitting procedure employed in [Stassun & Torres \(2016\)](#), and was used in S2017. The stellar atmosphere models used here assume main-sequence surface gravity $\log g$ and solar metallicity as was done in S2017. Each stellar atmosphere model is initiated at the T_{eff} derived in Section 3.1. The multiple photometric observations are collected by querying *Vizier*, and cover a wide wavelength spectrum from the far-Ultraviolet at $\sim 0.15 \mu\text{m}$ to the far-Infrared at $\sim 22 \mu\text{m}$. The complete list of surveys queried can be found in S2017, Section 2.3.1. The resulting SED fits have a χ_{nu}^2 value associated with them that is calculated from the case of two fitted parameters. These values are listed in Table 2, along with the calculated bolometric flux.

3.3. Stellar Radius

The angular radius can be derived using a rearranged version of the Stefan-boltzmann law, accomplished by replacing the luminosity in equation 1 with the luminosity-flux relation given in equation 2. The resulting equation can be rearranged such that we get

$$\Theta = f_{\text{bol}}^{0.5} \sigma_{SB}^{-0.5} T_{\text{eff}}^{-2} \quad (3)$$

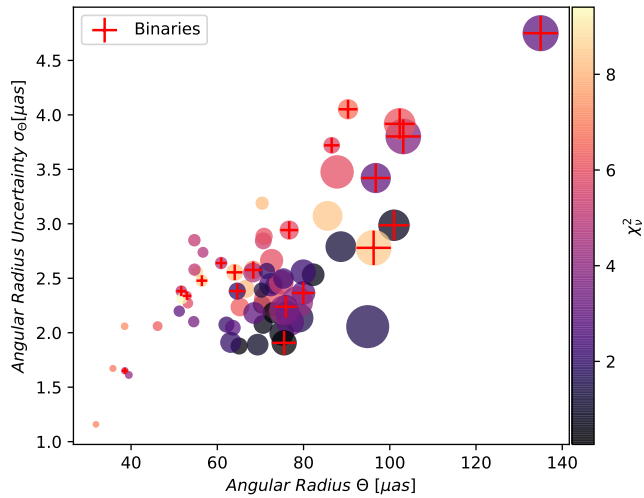


Figure 2. Plot of the angular radius uncertainty σ_{Θ} against the angular radius Θ . Both the x-axis and the y-axis are in units of microarcseconds. The points are colored according to the calculated χ^2_{ν} value of the SED fit. The size of the points are proportional to their $10^{10} \cdot F_{bol}$. The points with red crosses are identified binary stars.

where Θ is the angular radius, given by R_*/d . As we have already calculated the total bolometric flux, as well as the T_{eff} , we can simply calculate the angular radius for our Hyades Sample by inserting these values into equation 3. We list the resulting angular radii in units of milli-arcseconds in Table 2.

We plot the angular radius Θ against the angular radius uncertainty σ_{Θ} in Figure 2, where the points are sized by their bolometric flux, and colored by the calculated χ^2_{ν} of the SED fit. The stars with red crosses are the stars identified as binaries within our sample. Our calculated angular radii range for our identified single stars have a range of [35-100] μas with an average error on the calculated angular radius of $\sim 2.5 \mu\text{as}$. Overall, the small magnitude of the angular radius error, along with the relatively small values of χ^2_{ν} indicate that the SED fits are accurate.

To get the stellar radius from the angular radius, we can multiply the angular radius Θ of a star by its distance from us. The distance to the Hyades has been found to be about $46.75 \pm 0.46 \text{pc}$ (Gaia Collaboration, et al. (2017), using TGAS data from Gaia DR1). S2017 employed a single star cluster distance measurement for the Pleiades to convert their angular radii derivations to stellar radii, with an uncertainty added to the distance to reflect the depth of the Pleiades cluster.

With the recent release of the Gaia DR2 parallaxes (citation), we now have individual parallax measurements with very high precision ($\sigma_{\text{plx}} \sim 1 \times 10^{-4} (")$) for our entire Hyades sample. We convert these measured parallaxes in milli-arcseconds to distances in parsec by inverting the measured parallax values. We then derive the observed stellar radii by multiplying our individual angular radii values by the associated individual distances we have for the Hyades stars. We list these stellar radii values in units of R_{\odot} in Ta-

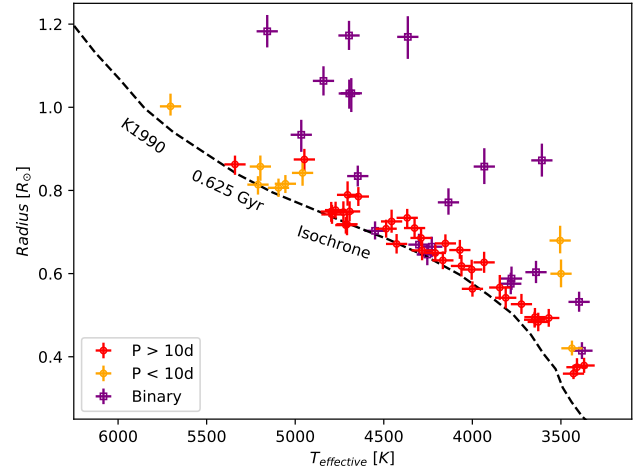


Figure 3. Plot of the calculated stellar radii for the Hyades stars against their calculated T_{eff} values. The vertical and horizontal error bars are the error on the calculated stellar radius, and T_{eff} , respectively. The red points are stars with measured rotation periods greater than 10 days, and the orange points are stars with measured rotation periods less than 10 days. The purple points are the identified binaries within the sample. The dashed black line is the fitted k1990 isochrone with a cluster age of 625 Myr.

ble 2.

Within the calculated stellar radii are a number of previously calculated, or derived parameters which have their associated errors. These parameters include derived T_{eff} , the total bolometric flux, and the distances of each star. The relative error contribution to the stellar radii is dominated by the angular radii error, as can be seen in Figure 4. Furthermore, since the calculation of the angular radii relies on the bolometric flux, which is derived from an SED fit based on our calculated T_{eff} value, the overall error within the angular radii derivation is dominated by T_{eff} .

It is easier to compare the fractional error, as it scales the two parameters. For the fractional distance errors, we find an average of 0.66 % and 0.4 % errors on the total sample, and the single star sample of Hyads, respectively. For the fractional angular radii error we find an average of 3.6 % and 3.5 % errors on the total sample, and single star sample of Hyads, respectively.

3.4. Calculating Radius Inflation

In order to determine if a star has a larger radius than expected, we compare our derived values to stellar isochrones from the literature. Isochrones are frequently used to predict theoretical properties of stellar populations under the assumption that they are all the same age and composition. In modeling the Hyades, we decide to use isochrones generated by Somers & Pinsonneault (2014) with a cluster age of 625 Myr and a metallicity of $[\text{Fe}/\text{H}] = 0.13$. We plot this isochrone alongside our Hyades sample in Figure 3.

Calculating the amount of radius inflation occurring with a particular star requires the measured stellar radius, and the expected stellar radius based on T_{eff} from a representative isochrone. To calculate the isochronal stellar radius, R_{iso} , a spline is fitted to the isochrone relating radius and T_{eff} .

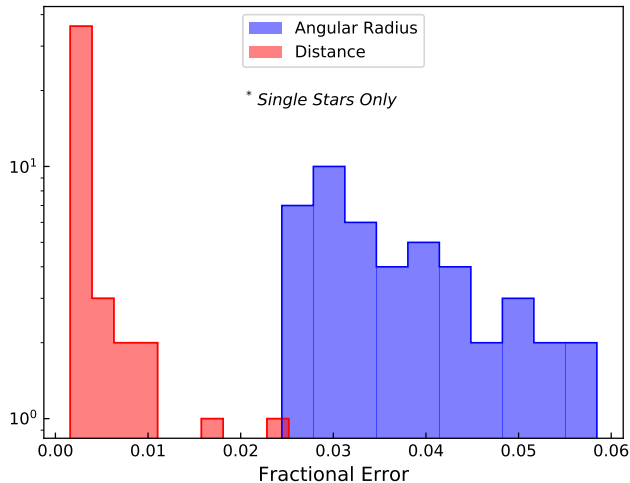


Figure 4. Plot of the fractional errors (variable error / variable) for the Gaia DR2 distances (Red) and the derived angular radii (Blue) of single stars in our Hyades Sample.

Then R_{iso} is calculated for a particular star by using the fitted spline to calculate the radius at its calculated T_{eff} . This was the method employed in calculating R_{iso} for the Pleiades in S2017 (see their section 3.3).

We introduce a new method for calculating the expected stellar radius R_{iso} for a star at a measured T_{eff} . Observational results show that radius inflation of $\sim 10\%$ is accompanied by a decline in T_{eff} of approximately half this percentage (e.g. [Stassun et al. 2012](#)). It is therefore important to account for this effect when establishing the model radius we compare to the observed radius. Consequently, we employ a method which finds R_{iso} for a particular star by moving within radius- T_{eff} parameter space bi-linearly from the observed stellar radius to R_{iso} following an equation relating fractional changes between T_{eff} , and radius. This relation can be written as follows:

$$\frac{dR}{R} = -\frac{2dT_{eff}}{T_{eff}} \quad (4)$$

Equation 4 can be derived from equation 1 with the imposed constraint that the change in luminosity, dL , be zero. The full derivation can be found within the appendix of this work.

Physically, equation 4 can be said to represent how a star increases(decreases) fractionally in radius for fractional decreases(increases) in its T_{eff} . If a star is undergoing radius inflation, the T_{eff} we observe from the V - K_s color is lower than it would be were it not inflated (citation), and we thus the isochronal radius at the measured T_{eff} is not the appropriate comparison value. Instead, R_{iso} must be found by finding the T_{eff} at which the star in question would lie on the isochrone *were it not inflated*. This relation is approximately linear for small enough changes in either radius or T_{eff} .

For each Hyades star, we find whether the star's observed stellar radius lies above(below) the isochrone. Then we increment the T_{eff} in a step-wise fashion down(up) and recalculate the final radius after the change in T_{eff} using equation 4.

In order to maintain the linearity of the relation, we proceed in steps of 1×10^{-2} K. This process is iterated over until the calculated T_{eff} is close enough to the T_{eff} from the isochrone line, which we take as the difference between the two T_{eff} values and impose a difference no greater than 1×10^{-3} K.

To visually illustrate how this procedure works, we plot a few selected stars in Figure 5(right panel) where the solid gray lines represent the calculation of R_{iso} from directly taking the same T_{eff} as we calculated in section 3.1. **The red step lines are not representative of the actual step-size used to get the T_{eff} without radius inflation.** As the step sizes we employed were 0.01 K, the overall step-wise behavior would look like a straight line. We also plot our entire sample and the newly calculated T_{eff} values in Figure 5(left plot), where the gray dot-dashed lines intersect the isochrone at the T_{eff} at which the stars would be, if there was no radius inflation. The symbol colors, and shapes of the left plot are the same as in Figure 3.

We can now proceed in calculating the radius inflation that might be taking place within the Hyades. We employ the same equation from S2017, which is written as:

$$\Delta R_* = \frac{R_* - R_{iso}}{R_{iso}} \quad (5)$$

Where R_* is the measured stellar radius we derived in section 3.3, and R_{iso} is the radius we calculated using isochrones, and the calibrated T_{eff} . Thus the ΔR_* value can be more simply stated as the fractional height above the fitted isochrone.

4. RESULTS

We list the calculated overall radius inflation, ΔR , for each star within our final sample in table 2. We also re-plot the color-magnitude diagram of the Hyades within Figure 6 to include the radius inflation information. Confirmed single stars within our sample are colored by the χ^2_ν values of the fitted SED and sized according to the calculated radius of inflation, using equation 5. Confirmed binary stars within the Hyades are plotted as red x's, and not sized according to their degree of radii inflation. S2017 showed how their properties affect the calculation of radius inflation, causing false signals of radius inflation. Within Figure 6 we see the presence of the binary main-sequence, as well as the location of two inflated single stars within this binary main-sequence. Single stars that have undergone radius inflation, are thought to exist within what is considered the binary main-sequence, and are incorrectly classified as photometric binaries. We will comment on this further with respect to our results in section 5.

4.1. Relationship to Rotation Period

As mentioned in §1, radius inflation may be connected to rapid rotation. We therefore consider the connection between radius inflation and stellar rotation, as was considered within the younger Pleiades open cluster in S2017, by looking at the observed rotation period of our Hyades sample and the radius inflation. In Figure 7 (left panel), we plot the observed rotation periods of our single stars against their calculated percentage of radii inflation. Overall we find that our Hyades sample periods are clustered around 10-15 days.

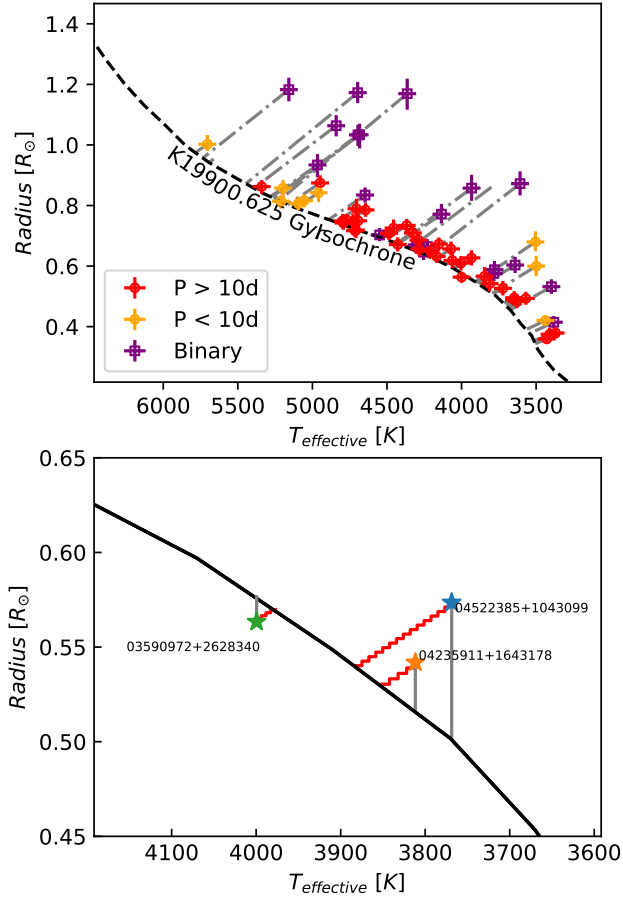


Figure 5. Top panel: Scatter plot of the slow rotating Hyads (yellow crosses), the fast rotating Hyads (red crosses), and the Hyades identified as binaries (purple crosses). Also plotted is the isochrone generated by K1990.625 . The gray dash-dotted lines show the difference in T_{eff} and radius between any one Hyad and its actual location on the isochrone. Bottom panel: Zoom-in of the top panel, in which we try to highlight the overall behavior of the DelR-DelT method with some example Hyads.

We bin the Hyades stars into two bins: the slow rotating stars (period > 10 days), and the fast rotating stars (period < 10 days). Within these two bins we find the average percentage of radius inflation and plot the two average values as the orange squares within Figure 7 (left panel). We also plot this sample by Rossby number (right panel), and bin them by either being slow ($R_0 > 2.5$) or fast ($R_0 < 2.5$)

We explore the degree of monotonicity between radius inflation and rotation period by calculating the Spearman’s Rank correlation coefficient, denoted by ρ_{spearman} , and the Kendall Tau correlation coefficient, denoted by τ_{kendall} . These coefficients describe the degree of correlation between two variables, where a value of 0 is no correlation, values > 0 are positive correlations, and values < 0 are negative correlations. In addition to the actual correlation coefficient, we calculate their p-values, to test against the null-hypothesis that these correlations could be due to random chance.

For period and delta radius, we calculate a value of $\rho_{\text{spearman}} = -0.0411$, and $\tau_{\text{kendall}} = -0.0283$, with p-values

of 0.788, and 0.784, respectively. This suggests that there is little to no correlation between period and radius inflation within this sample.

This result suggests that the rotation - radius inflation relation found by S2017 becomes undetectable via observed rotation periods or disappears as the cluster ages and the star’s magnetic fields become less active due to age related spin-down. To explore the likelihood of the second possibility, we consider also the Rossby number (Pizzolato et al. 2003) of the stars within the Hyades sample.

4.2. Relationship to Rossby Number

The Rossby number is the ratio of the rotation period of a star over the convective zone overturn time, denoted by τ_{cz} , which is a timescale to describe how long it takes convective motions to traverse the convective envelope. Noyes et al. (1984) argued that the Rossby number is the preferential metric to study magnetic activity because it appears to correlate with magnetic proxies such as Ca-II emission more strongly than just rotation itself.

In order to calculate the Rossby number for our Hyades sample, we employed the empirically calculated relationship between T_{eff} and the convective overturn time, τ_{cz} from Wright et al. (2011). We fit a cubic spline to this empirical relationship and calculated the expected convective overturn rate for our Hyades sample, using their individual T_{eff} from section 3.1. We calculate the Rossby number for our Hyades sample by dividing the rotation period of our stars by their calculated τ_{cz} value.

We plot the Hyades Rossby numbers against the calculated percentage of radius inflation in Figure 7(right panel). We see there there is a greater spread in the distribution of Rossby numbers within the Hyades sample than with period, indicative of the fact that most of the rapidly spinning stars are lower mass. We calculate the ρ_{spearman} and τ_{kendall} coefficients and attain values of -0.5376 and -0.3898, respectively. The associated p-value are both ~ 0.0001 . This indicates that there is significantly non-random negative trend between the Rossby number and the percentage of radius inflation.

5. DISCUSSION

We have employed several measures to ensure that our data is free of spurious values and that the relationship we have found between radius inflation and rotational period is not random. In the following section we discuss possible sources of error, and the impact of these sources of error on our findings within the Hyades cluster. The rest of the section will be dedicated to a discussion of our findings in the Hyades with respect to the findings of S2017 in the Pleiades. We will also discuss radius inflation as a function of age using these two clusters.

5.1. Potential Sources of Errors

5.1.1. Binaries

As discussed above, binaries are a potential source of radius inflation false-positives as the bolometric flux enhancement from the presence of a secondary would appear as higher luminosity – thus larger radius at fixed temperature

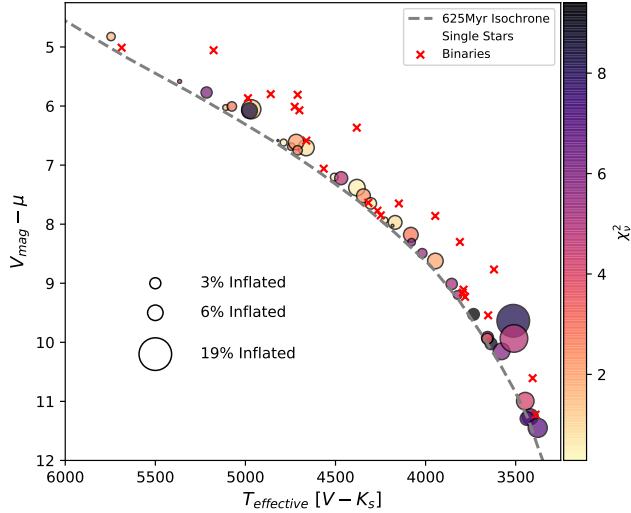


Figure 6. Temperature-magnitude diagram of the Hyades sample. The points are sized proportionally to their calculated $\Delta R_*/R_*$, and colored according to the χ^2 values for their SED fits. The gray dashed line is a 625Myr isochrone from a atmospheric model from Somers et. al. 2018 (In-prep).

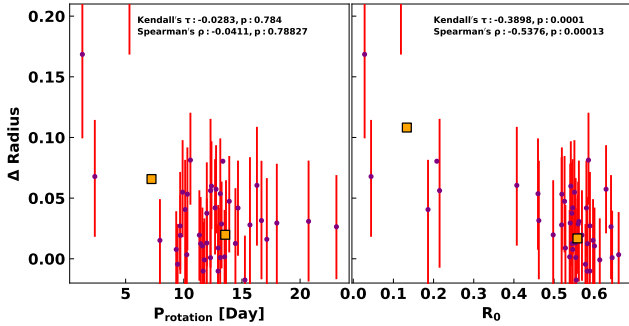


Figure 7. Left Panel: Plot of the measured rotation period of the Hyades final sample against the calculated percentage of radius inflation from Section 3.4. The purple points are the confirmed single stars. The orange squares are the average of the sample, binned into slow rotators ($p > 10$ d) and fast rotators ($p < 10$ d)

– in our analysis. While it is nearly impossible to prove that a star does not have a binary companion, we can assess how efficiently we have excluded binaries by comparing the derived radii of presumed-single and confirmed-binary stars rotating slower than $R_N \sim 0.1$. As these stars are not expected to be inflated by magnetic activity, stars with anomalously large derived radii can be confidently marked as binaries. S2017 did precisely this, finding significantly disparate distributions between the two samples. This provided confidence that most, if not all, binaries had been excluded from the full sample.

We repeat here this same exercise. In the top half of Fig. 8, we plot the periods of single stars with a rotation period greater than 10 days and binaries against their measured radius inflation. In addition to period, we plot the Rossby number of the same two sub-samples of stars against their measured radius inflation in the bottom panel of Figure 8. Like

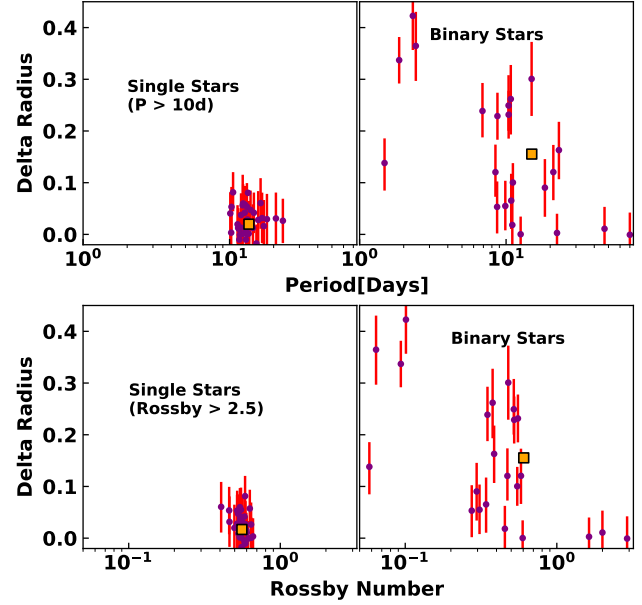


Figure 8. Top two panels: Plot of the period and ΔR for slow rotating single Hyades stars (left), and the confirmed binary stars (right). Bottom two panels: Plot of the Rossby number and ΔR for "slowly convective" (Rossby $> .25$) single stars (left) and the confirmed binary stars (right). The orange square in each of the four panel is the average of the plotted sample.

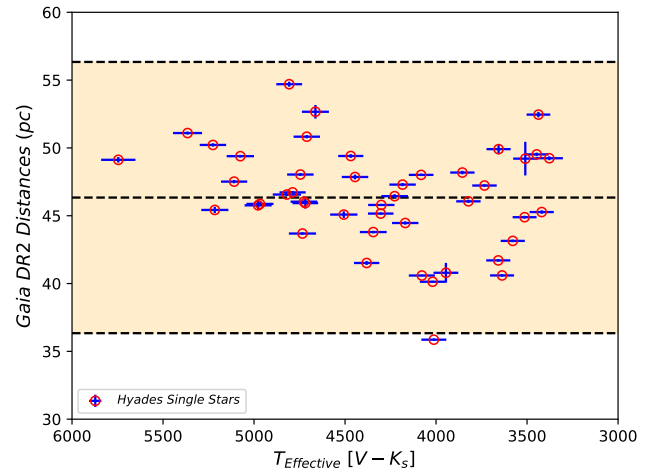


Figure 9. Plot of the T_{eff} against the calculated distances using Gaia DR2 parallaxes for the single stars in the Hyades. Error bars are included for both the distances and T_{eff} . The gray solid line at 46.75pc is the typically quoted distance to the center of the Hyades cluster. The two black horizontal dashed lines delineate the tidal radius of 10pc for the Hyades; this region has been shaded light orange.

S2017, we find that there is a significant contribution to calculated radius inflation due to binarity. We also find that in considering both rotation period, and Rossby number, that the distribution of slowly rotating single stars and binaries are different enough to claim here that we have effectively filtered out binaries from our Hyades sample.

5.1.2. Distance Errors

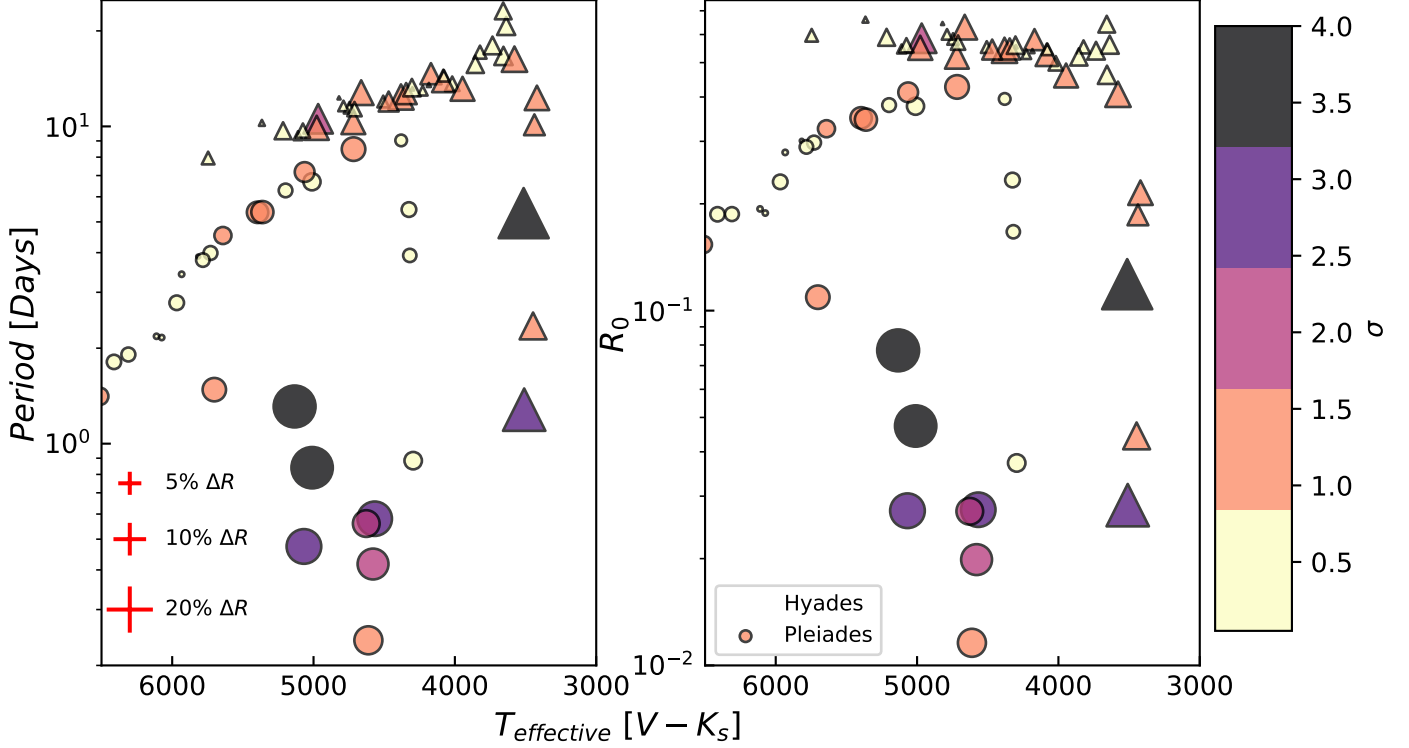


Figure 10. Left plot: Plot of the Rossby number and effective temperature for the Hyades single stars (triangles) and the Pleiades single stars (circles). Right plot: Plot of the rotation period and effective temperature for the Hyades single stars (triangles) and the Pleiades single stars (circles). All points within the two panels are sized proportionally to their calculated value of radius inflation. The three red crosses in the right panel serve as reference baselines. All points in the Hyades and Pleiades are colored according to the sigma significance of the calculated magnitude of radius inflation.

The calculation of the stellar radius, which is important as the baseline by which a star is judged to be radially inflated or not is vulnerable to either spurious distance measurements or high errors on the distance itself. High error arises from the typical employment of a cluster distance \pm cluster depth, where the cluster depth is then taken as the error on the distance of all the stars. For the Pleiades, this was taken to be $134 \text{ pc} \pm 3 \text{ pc}$ (from Soderblom et al. (2005)).

We are able to consider the individual distances to all of our Hyads with the Gaia DR2 catalog. The Gaia DR2 catalog measured proper-motions and parallaxes for over 10^9 stars down to a magnitude limit of $M_g \sim 20$, with parallax errors approaching $40 \mu\text{as}$. For our final sample of Hyades single stars, we find that the Gaia DR2 parallax errors span a range of $[37.8, 511.9] \mu\text{as}$ with an average of $86 \mu\text{as}$. Converting the parallax measurements to distances in parsecs we have an error on the individual distances of our single stars spanning the range $[0.065, 1.240] \text{ pc}$, with an average distance error of 0.186 pc . We have plotted the distances and T_{eff} for the single stars in our Hyades sample, along with the relevant errors in Figure 9.

The plotted single stars are all grouped around the typically quoted cluster distance to the Hyades of 46.75 pc (Reino et al. 2018). The scatter within this group exhibits the cluster depth along our line of sight, and is well within the typically cited tidal radius of the Hyades of $\pm 10 \text{ pc}$ (see Reino et al. (2018)).

From the Figure 9, as well as the relatively small contribution of distance errors shown in Figure 4, it is apparent that the distance measurements from Gaia DR2 for the Hyades are precise enough to employ for our conversion from angular radius to stellar radius.

5.2. Radius Inflation and Cluster Evolution: From the Pleiades to the Hyades

We now have two sets of measurements of radius inflation occurring within open clusters of different ages: The Pleiades cluster which has an estimated age of about 125 Myr, and the Hyades cluster which has an estimated age of 625 Myr. With this set of data covering a range of about 500 Myr we now have the opportunity to consider radius inflation in the broader sense of cluster evolution.

One of the aspects that need to be addressed in comparing the Hyades and Pleiades is the inherent mass difference we find between the samples. The Hyades cluster, being about 625 Myr old has spun down considerably more than the Pleiades. We find the effect of this spin down appear as a lower T_{eff} distribution when compared to the younger Pleiades (125 Myr). Our Hyads sample has an average T_{eff} of 4300 K while the Pleiades sample has an average T_{eff} of 5300 K. We test the similarity of these two distributions using the two sample KS test, finding a non-random difference between the two samples. We argue that this does not af-

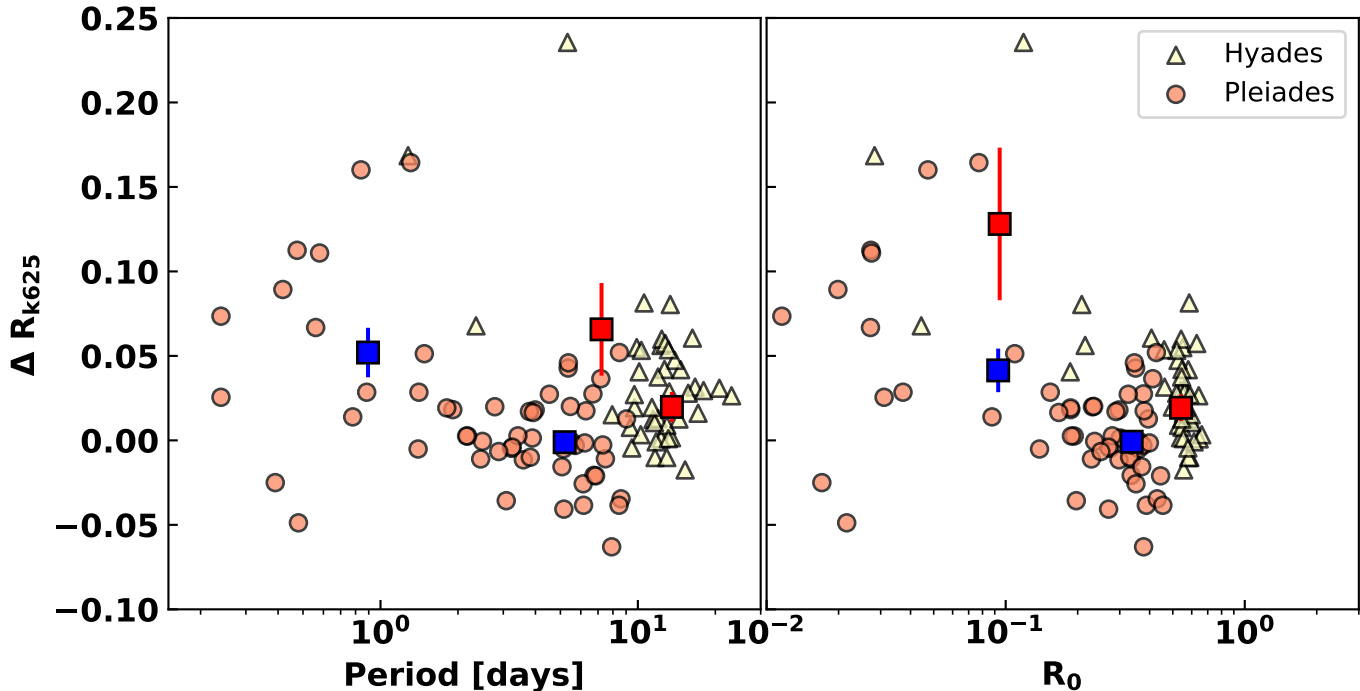


Figure 11. Left panel: Plot of Rossby number against ΔR for both the Hyades (triangles) and Pleiades (circles) single star samples. The two red squares are the mean values of ΔR for the low Rossby ($R_0 < 0.2$) bin and the high Rossby ($R_0 > 0.2$) bin of Hyades stars. The blue squares are means for the Pleiades stars, binned the same way. Right Panel: Rotation period plotted against ΔR for both the Pleiades (circles) and Hyades (triangles) samples. The blue and red squares correspond to means of the two bins within the Pleiades, and Hyades samples respectively. The Hyades is binned into slow rotators ($P > 10d$) and fast rotators ($P < 10d$). The Pleiades is binned into slow rotators ($P > 2d$) and fast rotators ($P < 2d$).

fect our results as presented, as we are comparing the overall presence of radius inflation as a function of cluster evolution here and not the relative degree of radius inflation.

In the right panel of Fig. 10, we plot the rotation rate of single stars in both the Pleiades (circles) and Hyades (triangles) against their T_{eff} . Each datum is colored according to its inferred radius inflation. As shown before, the stars with convincing evidence of inflation (darkest points) are rotating faster than average for their mass range. However, the inflated Hyades stars rotate slower than the inflated Pleiades stars. In the left panel, we show the same plot with the Rossby number substituted for rotation rate. As low-mass stars have a longer convective overturn timescale, the Rossby numbers of the inflated Hyades are similar to those of the faster-rotating Pleiads. In this panel, the inflated members of both cluster now occupy a similar range, namely $\lesssim 0.2$. That the onset of inflation seems more closely tied to Rossby number than raw rotation rate strongly suggests a link with magnetic properties.

An alternative way to view this data is shown in Figure 11. Here we plot the rotation rate and Rossby number of each star directly against the inferred radius inflation. While there seems to exist a connection between rotation and inflation in both clusters, in the sense that below a threshold rotation rate stars can show significant inflation, the transition rotation rate does not align for the two clusters. However, in Rossby space we see again an apparent transition around $R_N \sim 0.2$,

above which stars cluster around a low ΔR value, and above which stars may show large radius inflation values. The most likely explanation for this alignment is that the same magnetic mechanism is operating in both clusters, but sets in at different mass thresholds given the progressive spindown of stars with age.

Many previous studies have considered correlations between Rossby number and the magnetic properties of stars (Noyes et al. 1984; Pizzolato et al. 2003; Wright et al. 2011; Douglas, et al. 2014). A notable result is that around a Rossby number of 0.1-0.2, there is a break in correlation between rotation rate and magnetic proxies (e.g., $H\alpha$, X-rays, CaII H&K). Towards larger Rossby numbers, the magnetic proxies decrease in strength with decreasing rotation rate, but at lower Rossby numbers the correlation ceases, and the strength of magnetic proxies are approximately constant regardless of the rotation rate. A similar connection between Rossby number and starspot properties has also been noted (O’dell et al. 1995) SS17 noted that radius inflation set in around this Rossby value in the Pleiades, suggesting a connection. Fig. 11 shows that this Rossby threshold appears to hold in the much older Hyades as well, even though the low-Rossby stars are in a different mass range. This strongly suggests that the still-unclear physics of magnetic saturation are related to the onset of radius inflation at high rotation rate.

6. CONCLUSIONS

We have looked at radius inflation in single stars by continuing the work laid out in S2017 and applying it to the Hyades cluster. In this work we expand on the methods introduced by S2017, primarily with how the derived T_{eff} can be used to calculate the magnitude of radius inflation taking place. In this work we have taken into account the intrinsic relation between a star's radius and T_{eff} under the assumption that the star attempts to remain in equilibrium.

Radius inflation is the culmination of two processes that occur within stars: the differential rotation of the star, and the magnetic fields that are produced through the fluid motions within the convective layers in the star's interior. We compare the calculated percentage of radius inflation against the star's measured period of rotation as it is much more difficult to measure the magnetic fields within the star's interior.

We do not find a significant trend between the rotation period of our Hyades sample and the calculated radius inflation. We also consider the relation between the percentage of radius inflation and the Rossby number of the Hyades stars. The Rossby number is a well known metric that takes into

account the differential rotation and interior convective motions of the stars.

When we look at the relation between Rossby number and percentage of radius inflation, we do find a significant relation between the two. We also find that both the Pleiades sample and the Hyades sample experience more radius inflation below Rossby number of [0.1 - 0.2]. This suggests that the process of radius inflation takes place despite the spin-down that occurs with the evolution of a cluster.

KOJ and GS acknowledge the support of the Vanderbilt Office of the Provost through the Vanderbilt Initiative in Data-intensive Astrophysics (VIDA). KOJ thanks the LSSTC Data Science Fellowship Program, which is funded by LSSTC, NSF Cybertraining Grant #1829740, the Brinson Foundation, and the Moore Foundation; their participation in the program has benefited this work. KGS acknowledges NASA grant 17-XRP17 2-0024 for partial support. This research made use of the cross-match service provided by CDS, Strasbourg.

REFERENCES

- Aihara, H., Allende Prieto, C., An, D., et al. 2011, *ApJS*, 193, 29
 Cardelli, J. A., Clayton, G. C., & Mathis, J. S. 1989, *ApJ*, 345, 245
 Chabrier, G., Gallardo, J., & Baraffe, I. 2007, *A&A*, 472, L17
 Chambers, K. C., Magnier, E. A., Metcalfe, N., et al. 2016, arXiv:1612.05560
 Delorme, P., Collier Cameron, A., Hebb, L., et al. 2011, *MNRAS*, 413, 2218
 Douglas S. T., et al., 2014, *ApJ*, 795, 161
 Douglas, S. T., Agüeros, M. A., Covey, K. R., et al. 2016, *ApJ*, 822, 47
 Duchêne, G., Bouvier, J., Moraux, E., et al. 2013, *A&A*, 555, A137
 Fabricius C., Høg E., Makarov V. V., Mason B. D., Wycoff G. L., Urban S. E., 2002, *A&A*, 384, 180
 Feiden, G. A., & Chaboyer, B. 2013, *ApJ*, 779, 183
 Feiden, G. A., & Chaboyer, B. 2014, *ApJ*, 789, 53
 Gaia Collaboration, et al., 2017, *A&A*, 601, A19
 Goldman, B., Röser, S., Schilbach, E., et al. 2013, *A&A*, 559, A43
 Huang, Y., Liu, X.-W., Yuan, H.-B., et al. 2015, *MNRAS*, 454, 2863
 Jackson, R. J., & Jeffries, R. D. 2014, *MNRAS*, 441, 2111
 Jackson, R. J., & Jeffries, R. D. 2014, *MNRAS*, 445, 4306
 Jackson, R. J., Jeffries, R. D., Randich, S., et al. 2016, *A&A*, 586, A52
 Jackson, R. J., Deliyannis, C. P., & Jeffries, R. D. 2018, *MNRAS*, 476, 3245
 Johnson, H. L., & Knuckles, C. F. 1955, *ApJ*, 122, 209
 Kopytova, T. G., Brandner, W., Tognelli, E., et al. 2016, *A&A*, 585, A7
 Kurucz, R. L. 2013, *Astrophysics Source Code Library*, ascl:1303.024
 Lawrence, A., Warren, S. J., Almaini, O., et al. 2007, *MNRAS*, 379, 1599
 López-Morales, M., & Ribas, I. 2005, *ApJ*, 631, 1120
 Macdonald, J., & Mullan, D. J. 2010, *ApJ*, 723, 1599
 Martín, E. L., Lodieu, N., Pavlenko, Y., & Béjar, V. J. S. 2018, *ApJ*, 856, 40
 Mason B. D., Wycoff G. L., Hartkopf W. I., Douglass G. G., Worley C. E., 2001, *AJ*, 122, 3466
 Merilliod J.-C., Mayor M., Udry S., 2009, *A&A*, 498, 949
 Mullan, D. J., & MacDonald, J. 2001, *ApJ*, 559, 353
 Noyes, R. W., Weiss, N. O., & Vaughan, A. H. 1984, *ApJ*, 287, 769
 O'dell, M. A., Panagi, P., Hendry, M. A., & Collier Cameron, A. 1995, *A&A*, 294, 715
 Patience, J., Ghez, A. M., Reid, I. N., Weinberger, A. J., & Matthews, K. 1998, *AJ*, 115, 1972
 Pizzolato, N., Maggio, A., Micela, G., Sciortino, S., & Ventura, P. 2003, *A&A*, 397, 147
 Popper, D. M. 1997, *AJ*, 114, 1195
 Reino, S., de Bruijne, J., Zari, E., d'Antona, F., & Ventura, P. 2018, *MNRAS*, 477, 3197
 Roeser, S., Demleitner, M., & Schilbach, E. 2010, *AJ*, 139, 2440
 Skrutskie, M. F., Cutri, R. M., Stiening, R., et al. 2006, *AJ*, 131, 1163
 Skumanich, A. 1972, *ApJ*, 171, 565
 Soderblom, D. R., Nelan, E., Benedict, G. F., et al. 2005, *AJ*, 129, 1616
 Somers, G., & Pinsonneault, M. H. 2014, *ApJ*, 790, 72
 Somers, G., & Pinsonneault, M. H. 2015, *ApJ*, 807, 174
 Somers, G., & Pinsonneault, M. H. 2015, *MNRAS*, 449, 4131
 Somers, G., & Stassun, K. G. 2017, *AJ*, 153, 101
 Stassun, K. G., Kratter, K. M., Scholz, A., & Dupuy, T. J. 2012, *ApJ*, 756, 47
 Stassun, K. G., & Torres, G. 2016, *AJ*, 152, 180
 Torres, G., & Ribas, I. 2002, *ApJ*, 567, 1140
 Wenger, M., Ochsenbein, F., Egret, D., et al. 2000, *A&AS*, 143, 9
 Wright, N. J., Drake, J. J., Mamajek, E. E., & Henry, G. W. 2011, *ApJ*, 743, 48

Table 1. Observed Stellar Properties

2MASS	R.A.	Decl.	Distance (PC)	V_{mag}	$B - V$	$V - K_S$	P_{rot} (Days)	Binary?
03373495+2120355	54.3956	21.3432	45.87±0.13	9.362±0.008	0.92±0.004	2.240±0.021	10.57	No

Table 1 continued

Table 1 (*continued*)

2MASS	R.A.	Decl.	Distance (PC)	V_{mag}	$B - V$	$V - K_S$	P_{rot} (Days)	Binary?
03434706+2051363	55.946	20.86	45.27±0.13	14.54±0.008	0.9±0.004	4.927±0.023	12.3	No
03510309+2354134	57.7628	23.9037	40.88±0.08	10.118±0.008	1.2819±0.004	2.723±0.021	12.57	Yes
03524101+2548159	58.1708	25.8044	44.46±0.12	11.21±0.008		3.317±0.027	14.66	No
03550142+1229081	58.7559	12.4855	46.04±0.09	10.094±0.008	1.07±0.004	2.519±0.022	11.66	No
03583581+1306182	59.6492	13.105	61.35±0.19	8.951±0.008		1.576±0.022	22.26	Yes?
03590972+2628340	59.7905	26.4761	35.86±0.09	11.47±0.008		3.585±0.021	15.25	No
03591417+2202380	59.809	22.0439	40.6±0.08	13.066±0.008		4.362±0.018	20.73	No
04033902+1927180	60.9125	19.455	48.04±0.11	10.095±0.008	1.08±0.004	2.495±0.021	11.45	No
04052565+1926316	61.3568	19.4421	47.3±0.12	11.4±0.008	1.35±0.004	3.292±0.027	13.51	No
04063463+1332566	61.6443	13.549	49.91±0.38	13.409±0.008	1.47±0.004	4.318±0.019	16.68	No
04070122+1520062	61.7551	15.335	45.09±0.24	10.473±0.008	1.18±0.004	2.808±0.027	11.98	No
04074319+1631076	61.9299	16.5187	46.56±0.11	9.924±0.008	1.02±0.004	2.412±0.027	12.3	No
04081110+1652229	62.0462	16.873	40.13±0.07	11.51±0.008	1.44±0.004	3.577±0.025	13.63	No
04082667+1211304	62.1111	12.1918	46.44±0.15	11.269±0.008	1.33±0.004	3.223±0.028	12.96	No
04083620+2346071	62.1508	23.7686	47.52±0.12	9.41±0.008	0.9±0.004	2.087±0.016	9.35	No
04084015+2333257	62.1673	23.5571	46.08±0.17	12.861±0.008		4.332±0.025	21.02	Yes
04115620+2338108	62.9841	23.6363	40.29±1.15	9.392±0.008		2.982±0.025	2.309	Yes
04151038+1423544	63.7932	14.3984	48.01±0.09	11.585±0.008	1.38±0.004	3.457±0.018	13.91	No
04153367+1542226	63.8902	15.7062	45.58±0.14	10.931±0.008		3.077±0.024	47	Yes
04163346+2154269	64.1394	21.9074	51.1±0.11	9.125±0.008	0.81±0.004	1.849±0.024	10.26	No
04172512+1901478	64.3547	19.0299	47.86±0.18	10.8±0.008	1.22±0.004	2.891±0.024	12.95	No
04172811+1454038	64.3671	14.901	49.52±0.13	14.47±0.008	1.55±0.004	4.849±0.020	2.35	No
04174767+1339422	64.4486	13.6617	47.45±0.12	12.54±0.008		4.012±0.020	8.685	Yes
04175061+1828307	64.4609	18.4751	46.71±0.31	13.954±0.008		4.962±0.019	22.94	Yes
04175555+1432464	64.4814	14.5462	52.46±0.2	14.89±0.008		4.873±0.018	10.11	No
04181077+2317048	64.5449	23.2846	54.01±0.13	9.471±0.008		2.534±0.017	1.862	Yes
04223953+1816097	65.6647	18.2693	41.71±0.09	13.04±0.008		4.313±0.019	23.12	No
04232283+1939312	65.8451	19.6586	45.77±0.34	9.381±0.008	0.91±0.004	2.230±0.021	9.9	No
04232526+1545474	65.8552	15.7631	41.52±0.15	10.472±0.008	1.24±0.004	2.977±0.019	12.38	No
04235070+0912193	65.9612	9.20538	44.89±0.11	12.896±0.008	1.51±0.004	4.67±0.019	5.33	No
04235911+1643178	65.9963	16.7216	46.06±0.12	12.514±0.008	1.49±0.004	3.952±0.019	17.14	No
04241691+1800107	66.0704	18.0029	46.72±0.09	9.966±0.008	1.06±0.004	2.441±0.019	11.6	No
04250024+1659057	66.251	16.9849	54.7±0.19	10.248±0.008	1.03±0.004	2.417±0.017	11.77	No
04251456+1858250	66.3106	18.9736	52.95±0.2	12.728±0.008	1.48±0.004	4.022±0.019	10.84	Yes
04252501+1754552	66.3542	17.9153	46.91±0.09	11.128±0.008		3.151±0.019	70	Yes
04254754+1801022	66.448	18.0172	42.11±1.01	8.9889±0.008	0.94±0.004	2.221±0.022	8.46	Yes
04264825+1052160	66.701	10.8711	46.99±0.98	9.432±0.008	1.04±0.004	2.549±0.021	10.4	Yes
04272532+1415384	66.8555	14.2606	52.67±0.5	10.313±0.008	1.08±0.004	2.600±0.024	12.77	No
04274701+1425041	66.9459	14.4178	49.39±0.1	9.475±0.008	0.92±0.004	2.127±0.021	9.7	No
04275895+1830009	66.9956	18.5002	51.13±0.27	10.129±0.008		2.596±0.019	11.13	Yes
04282878+1741453	67.1199	17.6959	46.88±0.57	12.122±0.008	1.49±0.004	4.411±0.027	2.42	Yes
04303385+1444532	67.641	14.7481	50.0±1.14	14.72±0.008	1.56±0.004	5.008±0.019	18.41	Yes
04303486+1544023	67.6452	15.7339	57.14±0.88	8.84±0.008	0.84±0.004	2.022±0.019	8.73	Yes
04315244+1529585	67.9685	15.4995	45.79±0.08	11.0±0.008	1.31±0.004	3.105±0.025	13.13	No
04322565+1306476	68.1068	13.1132	46.79±0.1	11.0±0.008	1.19±0.004	3.346±0.021	1.48	Yes
04332699+1302438	68.3624	13.0455	43.14±0.09	13.328±0.008	1.57±0.004	4.505±0.020	16.29	No

Table 1 continued

Table 1 (*continued*)

2MASS	R.A.	Decl.	Distance (PC)	V_{mag}	$B - V$	$V - K_S$	P_{rot} (Days)	Binary?
04333716+2109030	68.4048	21.1508	43.8±0.09	10.726±0.008	1.23±0.004	3.040±0.027	12.69	No
04341113+1133285	68.5464	11.5579	47.84±0.49	11.25±0.008	1.39±0.004	3.191±0.030	11.03	Yes
04354850+1317169	68.9521	13.288	49.24±0.14	14.91±0.008	1.63±0.004	5.042±0.019	13.36	No
04360525+1541026	69.0218	15.684	50.22±0.12	9.345±0.008	0.87±0.004	1.972±0.016	9.47	No
04395095+1243426	69.9623	12.7285	43.69±0.09	9.992±0.008	1.07±0.004	2.512±0.024	10.85	No
04412780+1404340	70.3658	14.0761	49.21±1.24	13.395±0.008		4.683±0.022	1.28	No
04412876+1200337	70.3698	12.0093	47.23±0.09	12.898±0.008	1.5±0.004	4.144±0.021	18	No
04431568+1704088	70.8153	17.0691	45.93±0.4	9.92±0.008	1.0±0.004	2.524±0.017	10.31	No
04461879+0338108	71.5783	3.63636	45.16±0.08	10.922±0.008	1.27±0.004	3.096±0.021	13.25	No
04463036+1528194	71.6265	15.472	49.12±0.2	8.28±0.008	0.66±0.004	1.541±0.033	7.95	No
04471851+0627113	71.8271	6.45315	40.59±0.06	11.348±0.008	1.42±0.004	3.473±0.027	14.44	No
04480086+1703216	72.0036	17.056	44.15±0.88	11.085±0.008	1.41±0.004	3.711±0.024	10.77	Yes
04483062+1623187	72.1276	16.3885	48.18±0.13	12.427±0.008	1.47±0.004	3.884±0.018	15.69	No
04484211+2106035	72.1754	21.1009	45.43±0.23	9.057±0.008	0.85±0.004	1.985±0.019	9.69	No
04491296+2448103	72.304	24.8028	49.66±0.13	9.492±0.008	1.04±0.004	2.536±0.038	6.9	Yes
04500069+1624436	72.5028	16.4121	49.4±0.13	10.69±0.008	1.16±0.004	2.851±0.017	11.98	No
04510241+1458167	72.76	14.9713	40.79±0.73	11.675±0.008		3.708±0.021	13.14	No
04522352+1859489	73.098	18.9969	50.83±0.12	10.28±0.008	1.07±0.004	2.537±0.021	11.34	No
04522385+1043099	73.0994	10.7194	52.12±0.14	12.816±0.008		4.044±0.023	9.88	Yes?
05054038+0627545	76.4182	6.46515	65.51±1.39	9.88±0.008	0.95±0.004	2.362±0.022	10.41	Yes
05110971+1548574	77.7904	15.8159	57.0±2.31	12.08±0.008		3.977±0.018	14.94	Yes?

Table 2. Derived Stellar Properties ($V - K_s$)

2MASS	T_{eff} (K)	σ_{teff} (Systematic) (K)	\mathcal{F}_{bol} $\times 10^{-10}$ ($\text{erg cm}^{-2} \text{s}^{-1}$)	χ^2_{ν}	Angular Diameter $\times 10^{-2}$ (mas)	Radius (R_{\odot})	Δ Radius (%)
03373495+2120355	4967±14.29	60	62.8 $^{2.0}_{-2.52}$	1.22	8.8 $^{0.3}_{0.32}$	0.87 $^{0.03}_{0.03}$	8.1348 $^{3.677}_{3.907}$
03434706+2051363	3419±6.36	60	2.67 $^{0.245}_{-0.215}$	7.21	3.83 $^{0.23}_{0.21}$	0.37 $^{0.02}_{0.02}$	5.6189 $^{6.354}_{5.914}$
03510309+2354134	4565±11.71	60	36.5 $^{1.3599}_{-0.975}$	2.8	7.94 $^{0.29}_{0.27}$	0.7 $^{0.03}_{0.02}$	0.0261 $^{3.658}_{3.420}$
03524101+2548159	4169±12.35	60	19.6 $^{0.571}_{-0.547}$	0.95	6.98 $^{0.26}_{0.26}$	0.67 $^{0.03}_{0.03}$	4.1840 $^{3.931}_{3.907}$
03550142+1229081	4725±13.34	60	34.5 $^{1.97}_{-1.820}$	5.98	7.2 $^{0.3}_{0.29}$	0.71 $^{0.03}_{0.03}$	-1.014 $^{4.178}_{4.036}$
03583581+1306182	5686±20.52	60	71.5 $^{3.6400}_{-3.39}$	6.11	7.16 $^{0.27}_{0.26}$	0.94 $^{0.04}_{0.04}$	0.2782 $^{3.830}_{3.716}$
03590972+2628340	4012±8.59	60	18.2 $^{0.364}_{-0.527}$	1.18	7.26 $^{0.26}_{0.27}$	0.56 $^{0.02}_{0.02}$	-1.748 $^{3.508}_{3.656}$
03591417+2202380	3637±5.89	60	7.090 $^{0.4479}_{-0.458}$	8.71	5.51 $^{0.27}_{0.27}$	0.48 $^{0.02}_{0.02}$	3.0856 $^{4.960}_{5.008}$
04033902+1927180	4745±12.84	60	34.9 $^{1.66}_{-1.55}$	2.5	7.19 $^{0.28}_{0.27}$	0.74 $^{0.03}_{0.03}$	1.2464 $^{3.938}_{3.842}$
04052565+1926316	4183±12.45	60	15.5 $^{0.552}_{-0.524}$	2.04	6.16 $^{0.24}_{0.24}$	0.63 $^{0.02}_{0.02}$	0.1587 $^{3.908}_{3.867}$
04063463+1332566	3656±6.25	60	5.020 $^{0.29}_{-0.303}$	6.28	4.59 $^{0.21}_{0.22}$	0.49 $^{0.02}_{0.02}$	3.1523 $^{4.843}_{4.926}$
04070122+1520062	4506±14.91	60	28.80 $^{0.8029}_{-0.771}$	0.49	7.24 $^{0.26}_{0.26}$	0.7 $^{0.03}_{0.03}$	1.2973 $^{3.691}_{3.670}$
04074319+1631076	4819±17.5	60	39.5 $^{1.44}_{-1.69}$	5.32	7.41 $^{0.27}_{0.29}$	0.74 $^{0.03}_{0.03}$	0.0885 $^{3.707}_{3.873}$
04081110+1652229	4018±10.36	60	17.1 $^{0.8260}_{-0.917}$	5.33	7.01 $^{0.3}_{0.31}$	0.61 $^{0.03}_{0.03}$	1.9715 $^{4.341}_{4.502}$
04082667+1211304	4227±13.31	60	17.7 $^{0.33}_{-0.162}$	0.29	6.45 $^{0.23}_{0.23}$	0.64 $^{0.02}_{0.02}$	0.8891 $^{3.637}_{3.544}$
04083620+2346071	5109±11.96	60	55.89 $^{1.56}_{-1.49}$	1.55	7.84 $^{0.25}_{0.24}$	0.8 $^{0.03}_{0.03}$	0.7698 $^{3.178}_{3.151}$

Table 2 *continued*

Table 2 (continued)

2MASS	T_{eff} (K)	σ_{teff} (Systematic) (K)	\mathcal{F}_{bol} $\times 10^{-10}$ (erg cm $^{-2}$ s $^{-1}$)	χ^2_{ν}	Angular Diameter $\times 10^{-2}$ (mas)	Radius (R_{\odot})	Δ Radius (%)
04084015+2333257	3652±8.17	60	8.68 $^{0.534}_{-0.489}$	4.8	6.05 $^{0.29}_{0.28}$	0.6 $^{0.03}_{0.03}$	12.051 $^{5.435}_{5.256}$
04115620+2338108	4381±12.79	60	88.1 $^{2.73}_{-3.87}$	2.85	13.39 $^{0.49}_{0.53}$	1.16 $^{0.05}_{0.06}$	42.268 $^{6.604}_{6.965}$
04151038+1423544	4081±7.75	60	14.80 $^{0.669}_{-0.381}$	2.83	6.32 $^{0.25}_{0.23}$	0.65 $^{0.03}_{0.02}$	4.7376 $^{4.210}_{3.734}$
04153367+1542226	4317±11.8	60	21.29 $^{1.16}_{-1.08}$	7.22	6.78 $^{0.29}_{0.28}$	0.66 $^{0.03}_{0.03}$	1.0854 $^{4.356}_{4.239}$
04163346+2154269	5365±19.71	60	66.8 $^{1.29}_{-2.46}$	4.05	7.78 $^{0.24}_{0.27}$	0.85 $^{0.03}_{0.03}$	0.3351 $^{3.142}_{3.514}$
04172512+1901478	4445±12.66	60	21.8 $^{0.9770}_{-0.915}$	6.27	6.47 $^{0.26}_{0.25}$	0.67 $^{0.03}_{0.03}$	-1.014 $^{3.939}_{3.862}$
04172811+1454038	3446±5.68	60	2.900 $^{0.154}_{-0.123}$	4.14	3.93 $^{0.18}_{0.17}$	0.42 $^{0.02}_{0.02}$	6.7800 $^{4.967}_{4.665}$
04174767+1339422	3794±7.16	60	8.690 $^{0.581}_{-0.528}$	8.58	5.61 $^{0.27}_{0.26}$	0.57 $^{0.03}_{0.03}$	5.3209 $^{5.134}_{4.920}$
04175061+1828307	3405±5.28	60	4.979 $^{0.287}_{-0.264}$	5.82	5.27 $^{0.25}_{0.25}$	0.53 $^{0.03}_{0.02}$	16.299 $^{5.629}_{5.474}$
04175555+1432464	3437±5.16	60	1.870 $^{0.1750}_{-0.037}$	7.03	3.17 $^{0.19}_{0.12}$	0.36 $^{0.02}_{0.01}$	4.0565 $^{6.279}_{4.097}$
04181077+2317048	4710±10.37	60	66.1 $^{2.06}_{-1.97}$	0.81	10.04 $^{0.34}_{0.34}$	1.17 $^{0.04}_{0.04}$	33.699 $^{4.516}_{4.475}$
04223953+1816097	3658±6.26	60	7.02 $^{0.3}_{-0.282}$	3.41	5.42 $^{0.23}_{0.22}$	0.49 $^{0.02}_{0.02}$	2.6404 $^{4.322}_{4.257}$
04232283+1939312	4977±14.36	60	59.0 $^{2.0100}_{-3.13}$	8.35	8.49 $^{0.29}_{0.34}$	0.84 $^{0.03}_{0.03}$	5.4898 $^{3.712}_{4.287}$
04232526+1545474	4381±9.63	60	32.8 $^{0.6310}_{-0.912}$	0.6	8.17 $^{0.27}_{0.28}$	0.73 $^{0.02}_{0.03}$	5.9896 $^{3.539}_{3.696}$
04235070+0912193	3513±5.68	60	9.959 $^{0.7859}_{-0.591}$	8.15	7.0 $^{0.38}_{0.33}$	0.68 $^{0.04}_{0.03}$	23.553 $^{6.722}_{5.904}$
04235911+1643178	3822±6.95	60	8.42 $^{0.66}_{-0.591}$	5.06	5.44 $^{0.29}_{0.27}$	0.54 $^{0.03}_{0.03}$	1.6065 $^{5.347}_{5.045}$
04241691+1800107	4788±11.88	60	38.8 $^{0.6990}_{-0.679}$	0.65	7.44 $^{0.23}_{0.23}$	0.75 $^{0.02}_{0.02}$	1.0546 $^{3.174}_{3.167}$
04250024+1659057	4806±10.87	60	28.00 $^{1.01}_{-0.954}$	1.91	6.27 $^{0.22}_{0.21}$	0.74 $^{0.03}_{0.03}$	-0.087 $^{3.470}_{3.419}$
04251456+1858250	3789±6.81	60	7.25 $^{0.54}_{-0.485}$	4.89	5.14 $^{0.26}_{0.25}$	0.58 $^{0.03}_{0.03}$	6.5306 $^{5.478}_{5.193}$
04252501+1754552	4267±9.04	60	17.9 $^{0.9440}_{-1.01}$	8.25	6.36 $^{0.27}_{0.27}$	0.64 $^{0.03}_{0.03}$	-0.071 $^{4.175}_{4.294}$
04254754+1801022	4985±15.13	60	86.2 $^{3.0900}_{-4.8}$	3.69	10.23 $^{0.36}_{0.42}$	0.93 $^{0.04}_{0.04}$	12.037 $^{4.764}_{5.328}$
04264825+1052160	4700±12.55	60	67.1 $^{1.63}_{-3.82}$	6.11	10.16 $^{0.34}_{0.43}$	1.03 $^{0.04}_{0.05}$	24.931 $^{4.900}_{5.861}$
04272532+1415384	4662±14.19	60	29.8 $^{0.532}_{-0.518}$	0.91	6.88 $^{0.23}_{0.23}$	0.78 $^{0.03}_{0.03}$	5.7346 $^{3.635}_{3.629}$
04274701+1425041	5075±15.03	60	51.4 $^{0.9609}_{-1.39}$	2.81	7.62 $^{0.24}_{0.25}$	0.81 $^{0.03}_{0.03}$	1.9279 $^{3.167}_{3.320}$
04275895+1830009	4662±11.16	60	35.8 $^{1.06}_{-1.02}$	2.62	7.54 $^{0.26}_{0.25}$	0.83 $^{0.03}_{0.03}$	10.034 $^{3.776}_{3.750}$
04282878+1741453	3620±8.69	60	16.9 $^{1.0}_{-0.920}$	5.68	8.59 $^{0.41}_{0.4}$	0.87 $^{0.04}_{0.04}$	36.454 $^{6.773}_{6.588}$
04303385+1444532	3389±5.22	60	2.59 $^{0.134}_{-0.124}$	4.94	3.84 $^{0.18}_{0.17}$	0.41 $^{0.02}_{0.02}$	9.0356 $^{5.630}_{5.528}$
04303486+1544023	5176±14.26	60	87.4 $^{3.15}_{-2.99}$	8.41	9.56 $^{0.32}_{0.32}$	1.17 $^{0.04}_{0.04}$	22.881 $^{4.573}_{4.520}$
04315244+1529585	4300±12.22	60	19.9 $^{0.771}_{-0.904}$	8.11	6.61 $^{0.26}_{0.27}$	0.65 $^{0.03}_{0.03}$	0.1018 $^{3.885}_{4.062}$
04322565+1306476	4148±9.31	60	22.9 $^{1.5}_{-1.150}$	5.87	7.62 $^{0.36}_{0.32}$	0.77 $^{0.04}_{0.03}$	13.806 $^{5.330}_{4.763}$
04332699+1302438	3578±6.21	60	6.11 $^{0.3500}_{-0.322}$	5.88	5.29 $^{0.25}_{0.24}$	0.49 $^{0.02}_{0.02}$	6.0530 $^{4.968}_{4.823}$
04333716+2109030	4344±13.65	60	26.5 $^{0.758}_{-0.962}$	2.3	7.47 $^{0.27}_{0.29}$	0.7 $^{0.03}_{0.03}$	4.1978 $^{3.840}_{4.012}$
04341113+1133285	4248±14.58	60	17.80 $^{0.7159}_{-0.838}$	1.99	6.4 $^{0.26}_{0.27}$	0.66 $^{0.03}_{0.03}$	1.8194 $^{4.248}_{4.427}$
04354850+1317169	3377±nan	60	2.199 $^{0.147}_{-0.133}$	6.86	3.56 $^{nan}_{nan}$	0.38 $^{nan}_{nan}$	8.0417 $^{nan}_{nan}$
04360525+1541026	5225±12.6	60	55.79 $^{1.05}_{-2.02}$	4.13	7.49 $^{0.22}_{0.25}$	0.81 $^{0.02}_{0.03}$	-0.450 $^{2.930}_{3.309}$
04395095+1243426	4733±14.7	60	38.3 $^{0.684}_{-0.993}$	3.26	7.56 $^{0.25}_{0.26}$	0.71 $^{0.02}_{0.02}$	-25.53 $^{2.447}_{2.545}$
04412780+1404340	3509±6.49	60	6.42 $^{0.4870}_{-0.437}$	4.78	5.63 $^{0.3}_{0.29}$	0.6 $^{0.04}_{0.03}$	16.850 $^{6.921}_{6.639}$
04412876+1200337	3733±7.21	60	6.88 $^{0.468}_{-0.425}$	9.4	5.15 $^{0.26}_{0.24}$	0.52 $^{0.03}_{0.02}$	2.9473 $^{5.102}_{4.887}$
04431568+1704088	4718±10.41	60	41.7 $^{2.59}_{-1.609}$	2.13	7.95 $^{0.34}_{0.28}$	0.78 $^{0.03}_{0.03}$	5.3266 $^{4.628}_{3.854}$
04461879+0338108	4303±10.17	60	22.5 $^{0.634}_{-0.408}$	0.55	7.01 $^{0.25}_{0.24}$	0.68 $^{0.02}_{0.02}$	2.8709 $^{3.659}_{3.487}$
04463036+1528194	5745±34.28	60	127.0 $^{5.5100}_{-1.32}$	1.61	9.35 $^{0.37}_{0.31}$	0.99 $^{0.04}_{0.03}$	1.5176 $^{4.015}_{3.399}$
04471851+0627113	4077±11.7	60	18.2 $^{1.12}_{-1.02}$	5.98	7.03 $^{0.33}_{0.32}$	0.61 $^{0.03}_{0.03}$	1.2625 $^{4.734}_{4.555}$
04480086+1703216	3946±9.48	60	26.0 $^{1.89}_{-1.71}$	6.7	8.97 $^{0.45}_{0.43}$	0.85 $^{0.05}_{0.04}$	26.187 $^{6.863}_{6.579}$
04483062+1623187	3855±6.77	60	8.709 $^{0.7509}_{-0.727}$	5.15	5.44 $^{0.3}_{0.29}$	0.56 $^{0.03}_{0.03}$	2.7911 $^{5.691}_{5.581}$
04484211+2106035	5215±14.51	60	74.9 $^{2.98}_{-4.82}$	5.97	8.71 $^{0.3}_{0.38}$	0.85 $^{0.03}_{0.04}$	2.7088 $^{3.614}_{4.450}$

Table 2 continued

Table 2 (continued)

2MASS	T_{eff} (K)	σ_{teff} (Systematic) (K)	\mathcal{F}_{bol} $\times 10^{-10}$ (erg cm $^{-2}$ s $^{-1}$)	χ^2_{ν}	Angular Diameter $\times 10^{-2}$ (mas)	Radius (R_{\odot})	Δ Radius (%)
04491296+2448103	4726 \pm 25.52	60	60.6 $^{2.37}_{-2.96}$	2.95	9.55 $^{0.39}_{0.42}$	1.02 $^{0.04}_{0.04}$	23.869 $^{5.106}_{5.418}$
04500069+1624436	4468 \pm 9.16	60	24.5 $^{1.38}_{-1.27}$	4.67	6.79 $^{0.28}_{0.27}$	0.72 $^{0.03}_{0.03}$	3.7507 $^{4.350}_{4.197}$
04510241+1458167	3945 \pm 8.25	60	16.3 $^{0.655}_{-0.617}$	2	7.1 $^{0.28}_{0.28}$	0.62 $^{0.03}_{0.03}$	5.3628 $^{4.614}_{4.559}$
04522352+1859489	4710 \pm 12.61	60	30.4 $^{1.2200}_{-1.150}$	2.89	6.81 $^{0.25}_{0.25}$	0.74 $^{0.03}_{0.03}$	1.9499 $^{3.758}_{3.695}$
04522385+1043099	3780 \pm 8.15	60	7.040 $^{0.368}_{-0.406}$	2.92	5.08 $^{0.23}_{0.23}$	0.57 $^{0.03}_{0.03}$	5.4927 $^{4.706}_{4.878}$
05054038+0627545	4859 \pm 14.25	60	41.7 $^{0.4100}_{-0.404}$	0.26	7.49 $^{0.23}_{0.23}$	1.06 $^{0.04}_{0.04}$	23.153 $^{4.626}_{4.625}$
05110971+1548574	3809 \pm 6.58	60	13.69 $^{0.3629}_{-0.349}$	1.35	6.99 $^{0.26}_{0.26}$	0.86 $^{0.05}_{0.05}$	30.0777 $^{7.170}_{7.154}$

APPENDIX

A. DERIVATION OF RADIUS- T_{eff} RELATION

The derivation of equation 4 relies on the assumption that the luminosity of a star remains constant in spite of changes to either its T_{eff} , or its radius. We begin with the Stefan-Boltzmann equation of luminosity, which we re-write below:

$$L = 4\pi R_*^2 \sigma_{SB} T_{\text{eff}}^4 \quad (\text{A1})$$

We take the derivative of the above equation, relying on the product rule of derivatives to get the full expression, as written below:

$$\delta L = 8\pi R_* \delta R_* \sigma_{SB} T_{\text{eff}}^4 + 16\pi R_*^2 \sigma_{SB} T_{\text{eff}}^3 \delta T_{\text{eff}} \quad (\text{A2})$$

Next we divide both sides of equation A2 by the original Stefan-Boltzmann equation, which results in:

$$\frac{\delta L}{L} = \frac{8\pi R_* \delta R_* \sigma_{SB} T_{\text{eff}}^4}{4\pi R_*^2 \sigma_{SB} T_{\text{eff}}^4} + \frac{16\pi R_*^2 \sigma_{SB} T_{\text{eff}}^3 \delta T_{\text{eff}}}{4\pi R_*^2 \sigma_{SB} T_{\text{eff}}^4} \quad (\text{A3})$$

Equation A3 can be reduced by cancelling out all constants, as well as powers of radius, and T_{eff} which results in the following, simpler expression:

$$\frac{\delta L}{L} = \frac{2\delta R_*}{R_*} + \frac{4\delta T_{\text{eff}}}{T_{\text{eff}}} \quad (\text{A4})$$

Imposing our original assumption that $\delta L = 0$, we arrive at the following expression:

$$0 = \frac{2\delta R_*}{R_*} + \frac{4\delta T_{\text{eff}}}{T_{\text{eff}}} \quad (\text{A5})$$

Which can be rearranged and further reduced to our final expression for the relationship between fractional changes of radius, and T_{eff} :

$$\frac{dR}{R} = -\frac{2dT_{\text{eff}}}{T_{\text{eff}}} \quad (\text{A6})$$